Synthetic Metals 161 (2011) 1618–1622

Contents lists available at ScienceDirect

Synthetic Metals

journal homepage: www.elsevier.com/locate/synmet

Polymer infrared photo-detector with high sensitivity up to 1100 nm

En-Chen Chen[a], Shin-Rong Tseng[b], Yu-Chiang Chao[b], Hsin-Fei Meng[b,*], Chih-Feng Wang[c], Wen-Chang Chen[c,**], Chian-Shu Hsu[d], Sheng-Fu Horng[a]

[a] Department of Electrical Engineering, National Tsing Hua University, Hsinchu 300, Taiwan, ROC
[b] Institute of Physics, National Chiao Tung University, Hsinchu 300, Taiwan, ROC
[c] Department of Chemical Engineering and Institute of Polymer Science and Engineering, National Taiwan University, Taipei 106, Taiwan, ROC
[d] Department of Applied Chemistry, National Chiao Tung University, Hsinchu 300, Taiwan, ROC

ARTICLE INFO

Article history:
Received 17 November 2010
Received in revised form 18 April 2011
Accepted 19 May 2011
Available online 17 June 2011

Keywords:
Polymer
Photo-detector
Low band-gap
Near infrared

ABSTRACT

We reported a low band-gap conjugated polymer, poly[2,3-bis(4-(2-ethylhexyloxy)phenyl)-5,7-di(thiophen-2-yl)thieno[3,4-*b*]pyrazine] (PDTTP), was studied for the near infrared (NIR) photo-detector application. PDTTP shows intense absorption in NIR wavelength (to 1000 nm) and the estimated optical and electrochemical band-gaps of PDTTP are quite small around 1.15 eV and 1.08 eV, respectively. The low band-gap and the extended long wavelength absorption originates from the introduction of alternating TP units when its parent polythieno[3,4-*b*]pyrazine shows excellent narrow band-gap properties. Therefore, the relatively low band-gap and intense absorption in long wavelength of PDTTP make itself a promising candidate for near-infrared photo-detector. The hole mobility of the PDTTP measured from the bottom contact field effect transistor is around 1.40×10^{-3} cm^2/V s with a on/off ratio of 2100. The photo-detector based on bulk hetero-junction PDTTP and (6,6)-phenyl-C61-butyric acid methyl ester blend (PCBM) has the incident photon-to-electron conversion efficiency 28.9% at 1000 nm (−5 V) and 6.2% at 1100 nm (−5 V). This photo-detector can be operated at a high-speed of 1 MHz. The experimental result suggests the potential applications of low band-gap conjugated polymers on near-infrared photo-detectors.

1. Introduction

Conjugated polymer-based photo-detectors have the unique properties such as large area fabrication, low cost solution process and high sensitivity. Such properties are highly desirable to develop the high density array of distance proximity sensors, which combine polymer light-emitting diodes light source and polymer photo-detectors [1,2]. In order to achieve large detection distance, the operation of the proximity sensor in the infrared range is required to reduce the Rayleigh scattering from the detected object and the background noise. We have reported a detection up to 19 cm by a polymer near-infrared proximity sensor operated in the range from 700 nm to 850 nm [2]. The operation needs to be further moved to longer wavelength range, up to 1000 nm, to avoid the indoor lighting noise. Such high sensitivity proximity detection is especially important for the applications in fast moving machines such as cars or robots which move in the unstructured or unpredictable environments [3,4].

The most common way to achieve near infrared photo-detector is to use a low band-gap polymer as an electron donor blending with an electron acceptor like (6,6)-phenyl-C61-butyric acid methyl ester (PCBM). The low band-gap polymer can be achieved by hybridization of the energy levels of donor and acceptor fragments, leading to a donor–acceptor complex with narrow electron affinity (EA) and ionization potential (IP) energy separation. Donor–acceptor conjugated polymers have attracted extensive interest recently because their electronic and optoelectronic properties could be efficiently manipulated by intramolecular charge transfer. Many low band-gap polymers with the absorption larger than 900 nm have been synthesized for photovoltaic application [5–20]. Most of them have poor power conversion efficiency (PCE) and incident photon-to-electron conversion efficiency (IPCE) in photovoltaic application. Although the device structure of the photo-detector is the same as that of the solar cell, there are few discussions about their characteristics in the infrared photo-detectors based on low band-gap polymers since [21,22]. Unlike the photovoltaic, for photo-detector application, the devices are operated under reverse bias, and the IPCE may be enhanced in this condition.

In this study, a low band-gap donor–acceptor polymer, poly[2,3-bis(4-(2-ethylhexyloxy)phenyl)-5,7-di(thiophen-2-yl)thieno[3,4-*b*]pyrazine] (PDTTP), was synthesized and applied for the near infrared photo-detector. PDTTP shows not only

* Corresponding author. Tel.: +886 5731955..
** Corresponding author.
E-mail addresses: meng@mail.nctu.edu.tw (H.-F. Meng), chenwc@ntu.edu.tw (W.-C. Chen).

0379-6779/$ – see front matter © 2011 Elsevier B.V. All rights reserved.
doi:10.1016/j.synthmet.2011.05.027

intense absorption in near infrared wavelength (to 1000 nm) but also small band-gap around 1.15 and 1.08 eV, estimated from optical or electrochemical characteristics, respectively. A near infrared photo-detector based on the bulk hetero-junction system of PDTTP and PCBM blend is fabricated with response up to 1100 nm and operation speed up to 1 MHz. Our experimental results showed that the incident photon-to-electron conversion efficiency of the PDTTP:PCBM device was 28.9% at 1000 nm (−5 V) and 6.2% at 1100 nm (−5 V).

2. Experimental

2.1. Materials

1,1,1,2,2,2-Hexabutyldistannane, bis(triphenylphosphine)-dichloropalladium (II) ($PdCl_2(PPh_3)_2$), phenyl boronic acid, and bromobenzene were purchased from Aldrich (Missouri, USA) or Arcos (Geel, Belgium) and used without further purification. Ultra-anhydrous solvents used in the reaction were purchased from Tedia (Ohio, USA). The monomer, 5,7-bis(5-bromothiophene-2-yl)-2,3-bis(4-(2- ethylhexyloxy)phenyl)thieno[3,4-*b*]-pyrazine, were synthesized according to the similar procedures reported in the literature [23].

2.2. Polymer structure of PDTTP

The PDTTP was synthesized by Stille coupling reaction and the detailed polymerization was described in supporting information. The ^{1}H NMR spectrum of the PDTTP, as shown in Fig. S1, is consistent with the proposed structure. The weight-average molecular weight (M_w) is around 7900 and the polymer dispersion index (PDI) is about 1.65. The experimental elemental analysis result of the PDTTP is quite close to the theoretical contents except the carbon content and the deviation mainly arises from the end-group effect due to the low molecular weight. However, optical quality films could be obtained by spin-coating for device applications.

3. Characterization

^{1}H NMR spectrum was recorded by Bruker Avance DRX 500 MHz spectrometer in chloroform-d_1. Gel permeation chromatographic (GPC) analysis was performed on a Lab Alliance RI2000 instrument with two column, MIXED-C and MIXED-D from Polymer Laboratories) and instrument from Schambeck SFD Gmbh was used as a detector. All GPC analyses were manipulated on polymer/THF solution (2 mg/1 ml) at a flow rate of 1 ml/min at 40 °C and calibrated polystyrene standards. Elemental analysis was performed with a Heraeus varioIII-NCSH instrument.

UV–visible absorption spectra were recorded on a Jasco model UV/VIS/NIR V-570 spectrometer. For the solution spectrum, PDTTP was dissolved in THF (*ca.* 10^{-5} M) and then put in a quartz cell for measurement. As for the thin film spectra, PDTTP was first dissolved in THF (10 mg/ml) and filtered through 0.45 μm pore size PTFE membrane syringe filters, and then spin-coated at a speed rate of 1000 rpm for 60 s onto quartz substrate.

Cyclic voltammetry (CV) was performed in 0.1 M $TBAPF_6$ solution with the use of a three-electrode cell in which ITO (polymer films area about 0.5 cm × 0.7 cm) was used as a working electrode and a platinum wire was used as an auxiliary electrode. The scanning rate is 0.1 V s^{-1}. All cell potentials were taken with the use of a homemade Ag/AgCl, KCl (sat.) reference electrode. The energy levels of highest occupied molecular orbital (HOMO) were determined from the onset oxidation (E^{ox}_{onset}) and estimated on the basis of the reference energy level of ferrocence (4.8 V below the vacuum level) according to the following equation: HOMO $= -e(E^{ox}_{onset}) - E^{1/2}_{ferrocene} + 4.8$ (eV); lowest unoccupied molecular orbital (LUMO) $= -e(E^{red}_{onset} - E^{1/2}_{ferroscene} + 4.8)(eV)$ [24].

3.1. Field effect transistor (FET) devices [25]

Organic field-effect transistors (FETs) were prepared from polymer thin films with a bottom-contact configuration on the heavily n-doped silicon wafers, where 200 nm SiO_2 were thermally grown and used as the gate dielectric with a capacitance of 17 nF/cm^2. The aluminum was used to serve as the common bottom-gate electrode. The source/drain regions were defined by a 100 nm thick gold contact electrode through a regular shadow mask, and the channel length (L) and width (W) were 25 μm and 1000 μm, respectively. Afterward, the substrate was modified with octyltrichlorosilane (OTS) as silane coupling agents. 0.5 wt% polymer solutions in chlorobenzene was first filtered through 0.45 μm pore size PTFE membrane syringe filter, then spin-coated onto the silanized SiO_2/Si substrate at a speed rate of 1000 rpm for 60 s, and cured at 100 °C overnight under vacuum. The output and transfer characteristics of the FET devices were measured using Keithley 4200 semiconductor parametric analyzer. All the procedures and electrical measurements were performed in ambient air.

The typical p-channel characteristics (drain current (I_d) versus drain voltage (V_d) at various gate voltages (V_g)) when operate in the accumulation mode operation. In the saturation region ($V_d > V_g - V_t$), I_d can be described by Eq. (1):

$$I_d = \frac{WC_o\mu_h}{2L}(V_g - V_t)^2 \quad (1)$$

where μ_h is the hole mobility, W is the channel width, L is the channel length, and C_o is the capacitance of the gate insulator per unit area (SiO_2, 200 nm, C_o = 17 nF/cm^2), respectively. The saturation region mobility of the studied polymers is calculated from the transfer characteristics of TFT involving plotting $(I_d)^{1/2}$ versus V.

3.2. Polymer infrared photo-detector

The device structure of the photo-detector is ITO/PEDOT:PSS/PDTTP:PCBM/Ca/Al, which is the same with the photovoltaic device. ITO is indium tin oxide and PEDOT:PSS is poly-(3,4-ethylenedioxythiophene):poly-(styrenesulfonate) (CLEVIOS^{TM} P VP AI 4083, purchased from HC Starck). PCBM is purchased from Solenne. The ITO coated glass substrates are cleaned by ultrasonic bath for 20 min using acetone and subsequently rinsed three times by deionized water and then cleaned by UV ozone cleaner for 20 min. The PEDOT:PSS layer with 40 nm is spin coated at 2000 rpm on a pre-cleaned ITO substrate and baked at 200 °C in nitrogen for 15 min. PDTTP:PCBM blend is made with 1:1 weight ratio in dichlorobenzene solution with the concentration of 20 mg/ml. For the photovoltaic devices, the film thickness are 30 nm(700 rpm) and 120 nm(450 rpm). For the photo-detectors, the film thickness is 320 nm by drop casting. Ca(35 nm)/Al(100 nm) electrode is formed by thermal evaporation on top of the active layer. The active area of device is 4 mm^2. All the devices are packaged in the glove box and measured in the ambient environment. PCE is measured under AM 1.5 solar simulator (100 mW/cm^2) (XES-301S, SAN-EI). The IPCE is measured by the spectral response measurement system (SR300, Optosolar GMBH). For the transient response measurement, laser diode with 850 nm emission is driven by a function generator. The photo-current of polymer photo-detector is amplified by trans-impedanceamplifier

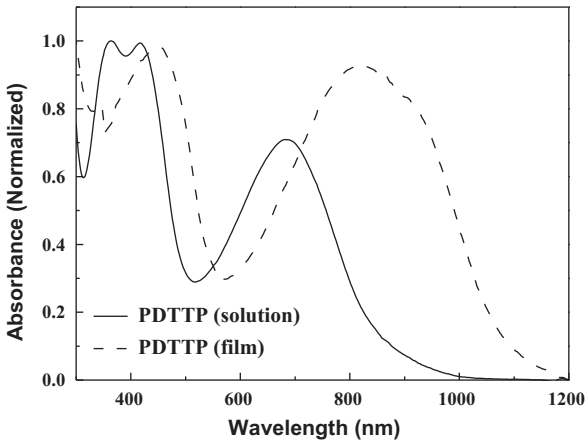

Fig. 1. Optical absorption spectrum of PDTTT in THF solution and as-cast film.

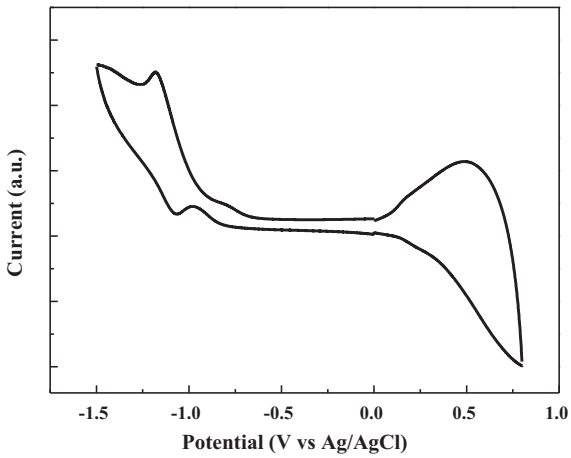

Fig. 2. Cyclic voltammogram of PDTTP thin film on ITO glass.

(DHPCA-100, Femto-tech Inc.) and the output signal is read from digital oscilloscope.

4. Results and discussion

4.1. Optical and electrochemical properties

The optical absorption spectra of PDTTP in THF solution and thin film state are shown in Fig. 1. The absorption maximums (λ_{max}) of PDTTP in solution are observed at 364 nm, 418 nm and 682 nm while the λ_{max} of PDTTP thin film state shows are appeared around 450 nm and 816 nm. Besides, as seen from the figure, the lowest energy absorption band in thin film state is broad, extending from 600 nm to 1000 nm with intense absorption where as that in solution is narrow and only extending from 500 nm to 800 nm. A substantial red shift of the absorption band in film state was due to the strong π–π intermolecular interactions of PDTTP. This is confirmed by the atomic force microscopy (AFM) images shown in Fig. S2 where aggregates of PDTTP are observed. The optical band gap (E_g^{opt}) of PDTTP estimated from the absorption band edge is about 1.15 eV. In comparison with parent polythiophene, the much lower band-gap of PDTTP demonstrates that the introduction of alternating TP units could efficiently extend the absorption to the long wavelength and reduce the band-gap due to the excellent small band-gap characteristic of parent polythieno[3,4-*b*]pyrazine [26,8]. The relatively low band-gap and intense absorption in long wavelength of PDTTP make itself a promising candidate for near-infrared photo-detector.

The ionization potential (IP, namely HOMO) and electron affinity (EA, namely LUMO) of the polymers were investigated by cyclic voltammetry (CV). Fig. 2 shows the oxidation and reduction behavior of PDTTP and both of them apparently exhibit quasi reversible properties. The energy levels of HOMO and LUMO were determined from the corresponding onset oxidation (E_{onset}^{ox}) or reduction (E_{onset}^{red}) according to the aforementioned equation. The estimated HOMO and LUMO levels of PDTTP are around −4.63 eV and −3.54 eV, respectively. As a result, the electrochemical band gap (E_g^{ec}) of PDTTP is 1.08 eV, which corresponds to the E_g^{opt} (1.15 eV) very well. In comparison, PDTTP has a similar structure to PTBEHT, in which the alkoxy chains are located on the *meta* position of the phenylene rings on the TP unit instead of *para* position, proposed by Janssen et al. [18]. Interestingly, from the above results, it could be found that the substituent on *para* position (PDTTP) shows stronger electron donation from the alkoxy group into the TP unit than on *meta* position (PTBEHT), which probably results from the high electron accepting strength of TP moiety [27].

4.2. Polymer thin film transistor and photovoltaic cell characteristics

Fig. 3 presents the transfer characteristic of PDTTP bottom-gate device. The estimated hole mobility of PDTTP is around 1.40×10^{-3} cm^2/V s with a on/off ratio of 2100. This high hole mobility can be attributed to the good backbone coplanarity formed by the incorporated TP segments as the other TP-based polymers described before [25]. Therefore, combined with the intense absorption band in near-IR region, the characteristics of high charge carrier mobility suggest PDTTP has greatly potential application for infrared photo-detector application.

The characteristic of photovoltaic devices based on the PDTTP:PCBM (1:1) blend are shown in Fig. 4. The thicknesses of active layer are 30 nm and 120 nm. The photovoltaic device with 30 nm active layer has the PCE of 0.07%, short circuit current (J_{SC}) of 1.13 mV/cm^2, open circuit voltage (V_{OC}) of 0.20 V and fill factor (FF) of 31%. The overall performances of the devices are low compared to the *ca.* 4–5% reached on poly(3-hexylthiophene):PCBM device [28–33]. This result is attributed to the low values of J_{SC} and V_{OC}. The low J_{SC} of PDTTP:PCBM is limited by the relatively low absorption coefficient of PDTTP, resulting in less efficient charge generation. The absorption coefficients of PDTTP:PCBM and P3HT:PCBM are shown in Fig. 4(b). For the PDTTP:PCBM, the absorption coefficients below 650 nm is low than that of P3HT:PCBM for about four times. The V_{OC} is low because of the low difference between the IP of PDTTP and EA of PCBM [34]. Therefore, not only absorption coefficient, but also the EA and IP values should be optimized when synthesizing new low band-gap polymer for the photovoltaic application.

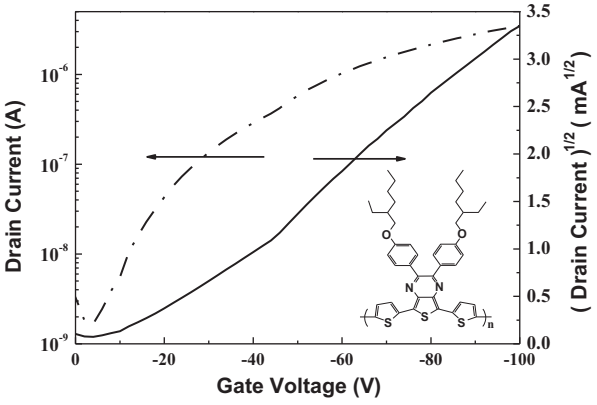

Fig. 3. Transfer characteristics of PDTTP based field-effect transistor device.

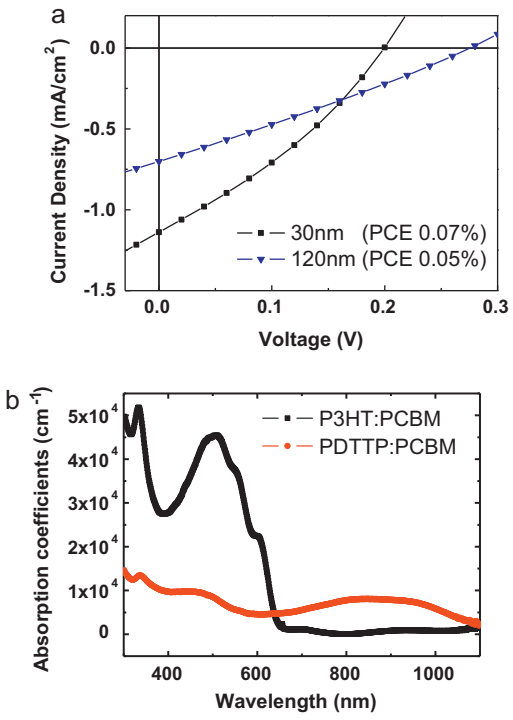

Fig. 4. (a) *J–V* characteristics of PDTTP:PCBM device with different thickness. (b) The absorption coefficients of PDTTP:PCBM and P3HT:PCBM layers.

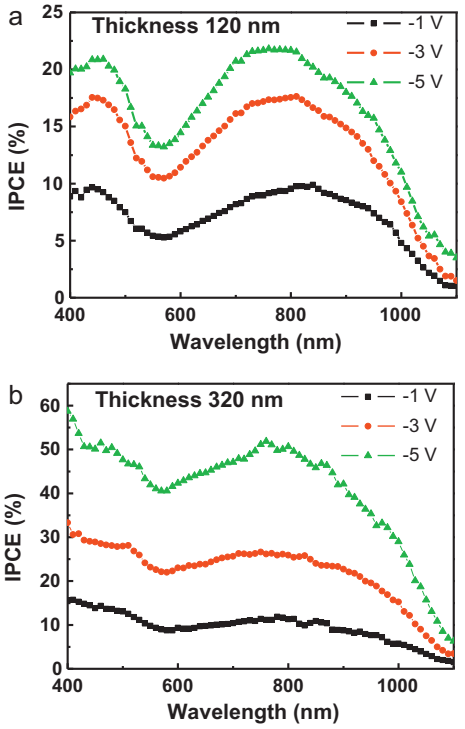

Fig. 5. IPCE of the near infrared photo-detector with (a) 120 nm, and (b) 320 nm active layer at various reverse biases.

4.3. Photo-detector device application

The requirement for the low band-gap polymers in the infrared photo-detector application is not so critical due to the face that the operation of photo-detectors is under reverse bias. The performance of the near infrared photo-detector based on PDTTP:PCBM blend as the active layer is discussed as below. Fig. 5(a) shows the IPCE of the photo-detector with a 120 nm active layer. As can be seen the device exhibits infrared response up to 1100 nm. The IPCE value of 810 nm is 9.7% at the reverse bias of 1 V and increases to 21.5% at the reverse bias of 5 V. The IPCE value of 1000 nm is only 11% at the reverse bias of 5 V, indicating the insufficient absorption of the PDTTP:PCBM layer with the thickness of 120 nm. The IPCE can be enhanced by increasing the thickness of active layer to 320 nm, shown in Fig. 5(b). The IPCE value shows 49.6% at 810 nm and remains 28.9% at 1000 nm as well as 6.2% at 1100 nm under the reverse bias of 5 V. The great enhancement of IPCE with the 320 nm PDTTP:PCBM layer can be attributed to the enhancement of absorption of the active layer. Such great enhancement from the thick active layer also implies the high carrier mobility in PDTTP:PCBM layer.

The dark *J–V* characteristics of the devices with thicknesses of 120 nm and 320 nm are shown in Fig. 6. The current density at 5 V is 163.2 and 26.4 mA/cm^2 for 120 and 320 nm devices, respectively. The rectifications in the dark between 5 V and −5 V are 49 and 11 for 120 and 320 nm devices, respectively. Such low rectification is due to the large reverse current, resulting from the electron injection from anode to the EA of PCBM or the hole injection from the cathode to the IP of PDPPT under large reverse bias. Due to Fermi level pinning effect, PEDOT:PSS and Ca/Al will respectively favor ohmic contact to the PDTTP and PCBM [35]. Therefore the barrier of holes and electrons in PDTTP:PCBM blend are about 0.9 eV, which is smaller than that in poly(3-hexylthiophene) (P3HT):PCBM (1.4 eV). Such dark reverse currents would reduce the sensitivity of the photo-detector. Multilayer device structure with carrier blocking layers is required to further reduce the dark reverse currents in the future [36]. This method will increase the sensitivity of the photo-detector.

In addition to the sensitivity, fast response is required for the high-speed scanning in the large area photo-detector array. The frame rate of photo-detector array is limited by the speed of photo-detector. In addition, the high-speed photo-detector enables noise removal by AC mode operation. The frequency responses of the polymer photo-detector with thickness of 320 nm under revere bias are shown in Fig. 7. The 850 nm laser diode was used for excitation. The cutoff frequency is higher than 4 MHz. As shown in Fig. 7(b), the transient response of the polymer photo-detector at 1 MHz demonstrates the rise time and fall time are about 150 and 140 ns, respectively. The carrier mobility of 1 MHz operation could be estimated about 10^{-4} cm^2/V s by calculating the average drift velocity under the assumption of the uniform electric field in the active layer.

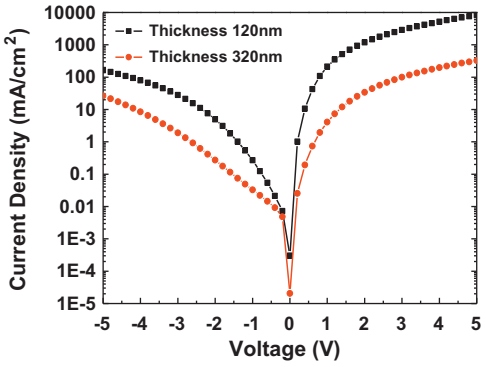

Fig. 6. *J–V* characteristics in the dark of the near infrared photo-detectors with 120 and 320 nm active layers.

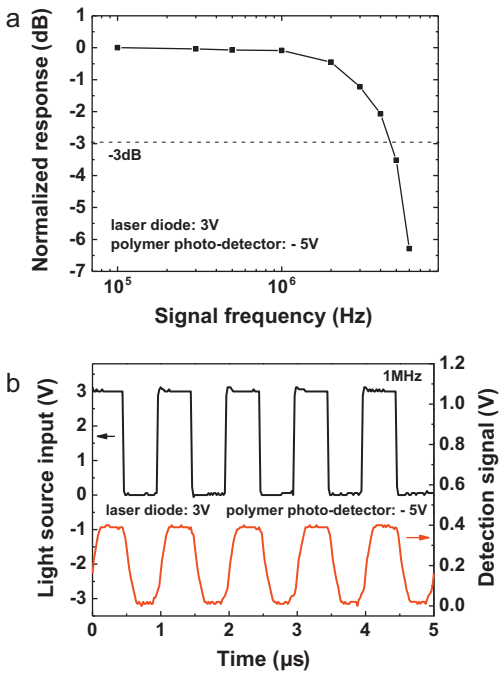

Fig. 7. (a) Frequency response of the near infrared photo-detector with 320 nm active layer. (b) Transient response of the near infrared photo-detector.

5. Conclusions

We have successfully prepared a low band-gap donor–acceptor conjugated polymer, PDTTP, for the near-infrared photo-detector application. This polymer has a optical band gap of 1.15 eV with the hole mobility up to 1.40×10^{-3} cm^2/V s. The near infrared photo-detector based on the blend of PDTTP:PCBM has good infrared response up to 1100 nm. Such device also shows fast response lager than 1 MHz. The new low band-gap polymer, PDTTP, is therefore a promising material for large-area and all-polymer distance sensor array application.

Acknowledgment

This work is supported by the National Science Council of Taiwan under grant number NSC97-2628-M-009-016 and NSC97-2120-M-007-004.

Appendix A. Supplementary data

Supplementary data associated with this article can be found, in the online version, at doi:10.1016/j.synthmet.2011.05.027.

References

[1] C.M. Yang, P.Y. Tsai, S.F. Horng, K.C. Lee, S.R. Tseng, H.F. Meng, J.T. Shy, C.F. Shu, Appl. Phys. Lett. 92 (2008) 083504.
[2] E.C. Chen, S.R. Tseng, J.H. Ju, C.M. Yang, H.F. Meng, S.F. Horng, C.F. Shu, Appl. Phys. Lett. 93 (2008) 063304.
[3] V.J. Lumelsky, M.S. Shur, S. Wagner, IEEE Sens. J. 1 (2001) 41.
[4] B.P. Rand, J. Xue, M. Lange, S.R. Forrest, IEEE Photonics Technol. Lett. 15 (2003) 1279.
[5] E. Perzon, X. Wang, F. Zhang, W. Mammo, J.L.D.P.D.L. Cruz, O. Inganäs, F. Langa, M.R. Andersson, Synth. Met. 154 (2005) 53.
[6] E. Perzon, X. Wang, S. Admassie, O. Inganäs, M.R. Andersson, Polymer 47 (2006) 4261.
[7] M.H. Petersen, O. Hagemann, K.T. Nielsen, M. Jorgensen, F.C. Krebs, Sol. Energy Mater. Sol. Cells 91 (2007) 996.
[8] L. Wen, B.C. Duck, P.C. Dastoor, S.C. Rasmussen, Macromolecules 41 (2008) 4576.
[9] J. Hou, H.Y. Chen, S. Zhang, G. Li, Y. Yang, J. Am. Chem. Soc. 130 (2008) 16144.
[10] W. Walker, B. Veldman, R. Chiechi, S. Patil, M. Bendikov, F. Wudl, Macromolecules 41 (2008) 7278.
[11] L. Goris, M.A. Loi, A. Cravino, H. Neugebauer, N.S. Saricifti, I. Polec, L. Lutsen, E. Andries, J. Manca, L.D. Schepper, D. Vanderzande, Synth. Met. 138 (2003) 249.
[12] X. Wang, E. Perzon, J.L. Delgado, P.D.L. Cruz, F. Zhang, F. Langa, M. Andersson, O. Inganäs, Appl. Phys. Lett. 85 (2004) 21.
[13] X. Wang, E. Perzon, F. Oswald, F. Langa, S. Admassie, M.R. Andersson, O. Inganäs, Adv. Funct. Mater. 15 (2005) 1665.
[14] B.P. Rand, J. Xue, F. Yang, S.R. Forrest, Appl. Phys. Lett. 87 (2005) 233508.
[15] X. Wang, E. Perzon, W. Mammo, F. Oswald, S. Admassie, N.K. Persson, F. Langa, M.R. Andersson, O. Inganäs, Thin Solid Films 511 (2006) 576.
[16] Y. Xia, L. Wang, X. Deng, D. Li, X. Zhu, Y. Cao, Appl. Phys. Lett. 89 (2006) 081106.
[17] E. Perzon, F. Zhang, M. Andersson, W. Mammo, O. Inganäs, M.R. Andersson, Adv. Mater. 19 (2007) 3308.
[18] M.M. Wienk, M.G.R. Turbiez, M.P. Struijk, M. Fonrodona, R.A.J. Janssen, Appl. Phys. Lett. 88 (2006) 153511.
[19] K.F. Cheng, C.L. Liu, W.C. Chen, J. Polym. Sci. Polym. Chem. 45 (2007) 5872.
[20] F. Zhang, J. Bijleveld, E. Perzon, K. Tvingstedt, S. Barrau, O. Inganäs, M.R. Andersson, J. Mater. Chem. 18 (2008) 5468.
[21] Y. Yao, Y. Liang, V. Shrotriya, S. Xiao, L. Yu, Y. Yang, Adv. Mater. 19 (2007) 3979.
[22] X. Gong, M. Tong, Y. Xia, W. Cai, J.S. Moon, Y. Cao, G. Yu, C.L. Shieh, B. Nilsson, A.J. Heeger, Science 325 (2009) 1665.
[23] W. Mammo, S. Admassie, A. Gadisa, F. Zhang, O. Inganäs, M.R. Andersson, Sol. Energy Mater. Sol. Cells 91 (2007) 1010.
[24] Q.J. Sun, H.Q. Wang, C.H. Yang, Y.F. Li, J. Mater. Chem. 13 (2003) 800.
[25] C.L. Liu, J.H. Tsai, W.Y. Lee, W.C. Chen, S.A. Jenekhe, Macromolecules 41 (2008) 6952.
[26] D.D. Kenning, S.C. Rasmussen, Macromolecules 36 (2003) 6298.
[27] A. Gadisa, W. Mammo, L.M. Andersson, S. Admassie, F. Zhang, M.R. Andersson, O. Inganäs, Adv. Funct. Mater. 17 (2007) 3836.
[28] C.H. Woo, B.C. Thompson, B.J. Kim, M.F. Toney, J.M.J. Fréchet, J. Am Chem. Soc. 130 (2008) 16324.
[29] M. Reyes-Reyes, K. Kim, D.L. Carroll, Appl. Phys. Lett. 87 (2005) 083506.
[30] G. Li, Y. Yao, H. Yang, V. Shorotriya, G. Yang, Y. Yang, Adv. Funct. Mater. 17 (2007) 1636.
[31] G. Li, V. Shrotriya, J. Huang, Y. Yao, T. Moriarty, K. Emery, Y. Yang, Nat. Mater. 4 (2005) 864.
[32] A.C. Mayer, S.R. Scully, B.E. Hardin, M.W. Rowell, M.D. McGehee, Mater. Today 10 (2007) 28.
[33] W. Ma, C. Yang, X. Gong, K. Lee, A. Heeger, J. Adv. Funct. Mater. 15 (2005) 1617.
[34] A. Gadisa, M. Svensson, M.R. Andersson, O. Inganäs, Appl. Phys. Lett. 84 (2004) 1609.
[35] C.J. Brabec, A. Cravino, D. Meissner, N.S. Sariciftci, T. Fromherz, M.T. Rispens, L. Sanchez, J.C. Hummelen, Adv. Funct. Mater. 11 (2001) 374.
[36] L. Chen, P. Degenaar, D.D.C. Bradley, Adv. Mater. 20 (2008) 1679.